A 1/f Noise Upconversion Reduction Technique for Voltage-Biased RF CMOS Oscillators

Shahmohammadi, Mina; Babaie, Masoud; Staszewski, Robert Bogdan

DOI
10.1109/JSSC.2016.2602214

Publication date
2016

Document Version
Final published version

Published in
IEEE Journal of Solid State Circuits

A 1/f Noise Upconversion Reduction Technique for Voltage-Biased RF CMOS Oscillators

Mina Shahmohammadi, *Student Member, IEEE*, Masoud Babaie, *Member, IEEE*, and Robert Bogdan Staszewski, *Fellow, IEEE*

***Abstract*— In this paper, we propose a method to reduce a flicker (1/f) noise upconversion in voltage-biased RF oscillators. Excited by a harmonically rich tank current, a typical oscillation voltage waveform is observed to have asymmetric rise and fall times due to even-order current harmonics flowing into the capacitive part, as it presents the lowest impedance path. The asymmetric oscillation waveform results in an effective impulse sensitivity function of a nonzero dc value, which facilitates the 1/f noise upconversion into the oscillator's 1/f^3 phase noise. We demonstrate that if the ω_0 tank exhibits an auxiliary resonance at $2\omega_0$, thereby forcing this current harmonic to flow into the equivalent resistance of the $2\omega_0$ resonance, then the oscillation waveform would be symmetric and the flicker noise upconversion would be largely suppressed. The auxiliary resonance is realized at no extra silicon area in both inductor- and transformer-based tanks by exploiting different behaviors of inductors and transformers in differential- and common-mode excitations. These tanks are ultimately employed in designing modified class-D and class-F oscillators in 40 nm CMOS technology. They exhibit an average flicker noise corner of less than 100 kHz.**

***Index Terms*— Class-D oscillator, class-F oscillator, digitally controlled oscillator, flicker noise, flicker noise upconversion, impulse sensitivity function (ISF), phase noise (PN), voltage-biased RF oscillator.**

I. Introduction

CLOSE-IN spectra of RF oscillators are degraded by a flicker (1/f) noise upconversion. The resulting low-frequency phase noise (PN) fluctuations can be mitigated as long as they fall within a loop bandwidth of an enclosing phase-locked loop (PLL). However, the PLL loop bandwidths in cellular transceivers are less than a few tenths to a few hundreds of kilohertz [1], [2], which is below the typical 1/f^3 PN corner of CMOS oscillators [3]–[5]. Consequently, a considerable amount of the oscillator's low-frequency noise cannot be filtered by the loop and will adversely affect the transceiver operation.

In a current-biased oscillator, flicker noise of a tail transistor, M_T, modulates the oscillation voltage amplitude and then upconverts to PN via an AM–FM conversion mechanism through nonlinear parasitic capacitances of active devices, varactors, and switchable capacitors [6], [7] [see Fig. 1(a)].[1] An intuitive solution is to configure the oscillator into a *voltage-biased* regime, which involves removing M_T [8], or replacing it with a tail resistor, R_T, in Fig. 1(b). Such expected PN reduction is highly dependent on the tail transistor's operating region. If M_T in Fig. 1(a) is always in saturation, the amount of 1/f noise is considerable, and the tail resistor R_T in Fig. 1(b) could improve the low-frequency PN performance, as shown in Fig. 1(c), However, in advanced CMOS process nodes with a reduced supply voltage, M_T partially enters the triode region, thereby degrading the oscillator's effective noise factor but improving the 1/f noise upconversion [see Fig. 1(d)]. In [3], class-C oscillators were designed with both a tail transistor and a tail resistor. Measured 1/f^3 corners are almost the same, thus supporting our discussion. However, regardless of the M_T operating region, removing this source would still not completely eliminate the 1/f noise upconversion.

Another mechanism of the 1/f upconversion is due to Groszkowski effect [9]. In a harmonically rich tank current,

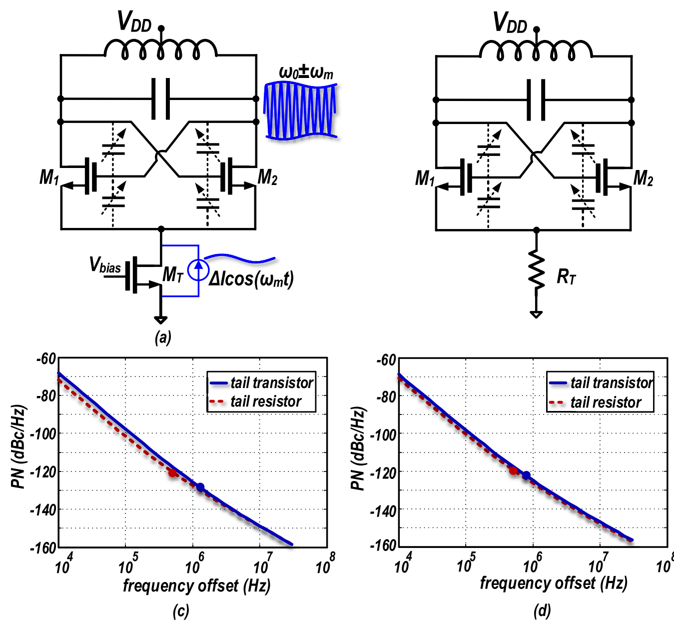

Fig. 1. Class-B oscillator (a) with tail transistor M_T and (b) with tail resistor R_T, and their PN when (c) M_T is always in saturation and (d) M_T partially enters into triode.

[1] It is shown in [6] that for certain values of varactor bias voltages, this upconversion is almost eliminated.

Manuscript received November 22, 2015; revised April 13, 2016; accepted August 10, 2016. Date of publication September 19, 2016; date of current version October 29, 2016. This paper was approved by Associate Editor Kenichi Okada. This work was supported in part by European Research Council (ERC) Consolidator Grant 307624 TDRFSP.

M. Shahmohammadi and M. Babaie are with the Department of Electrical Engineering, Delft University of Technology, 2628 CD Delft, The Netherlands (e-mail: m.shahmohammadi@tudelft.nl).

R. B. Staszewski is with School of Electrical and Electronic Engineering, University College Dublin, Dublin 4, Ireland, and also with Delft University of Technology, 2628 CD Delft, the Netherlands.

Color versions of one or more of the figures in this paper are available online at http://ieeexplore.ieee.org.

Digital Object Identifier 10.1109/JSSC.2016.2602214

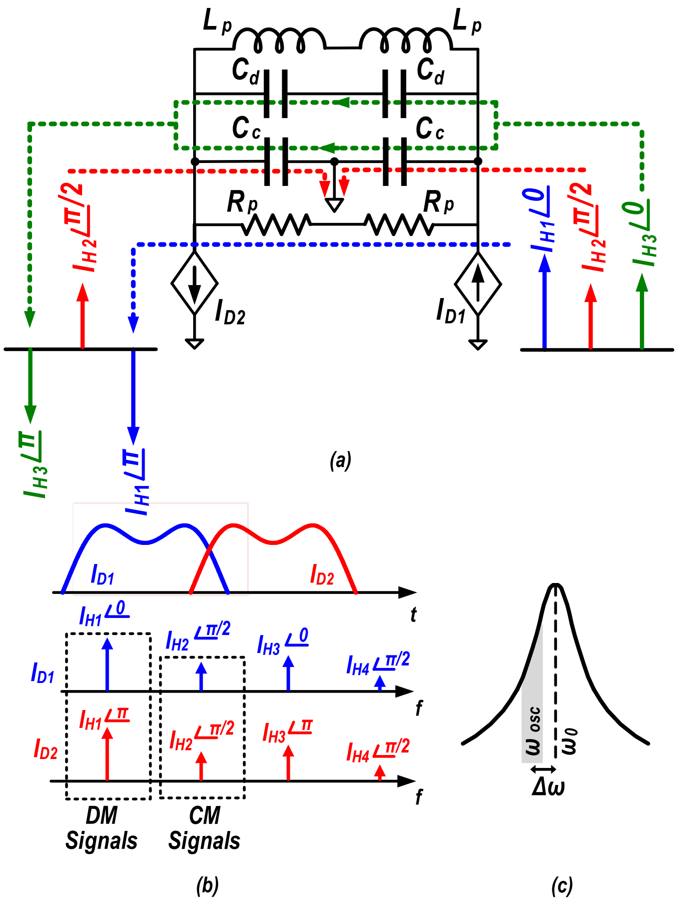

Fig. 2. (a) Current harmonics paths. (b) Drain current in time and frequency domains. (c) Frequency drift due to Groszkowski's effect.

the fundamental component, I_{H1}, flows into the equivalent parallel resistance of the tank, R_p. Other components, however, mainly take the capacitive path due to their lower impedance [see Fig. 2(a)]. Compared with the case with only the fundamental component, the capacitive reactive energy increases by the higher harmonics flowing into them. This phenomenon makes the tank's reactive energy unbalanced. The oscillation frequency will shift down from the tank's natural resonance frequency, ω_0, in order to increase the inductive reactive energy, and restore the energy equilibrium of the tank. This frequency shift is given by [10]

$$\frac{\Delta\omega}{\omega_0} = -\frac{1}{Q^2}\sum_{n=2}^{\infty}\frac{n^2}{n^2-1}\cdot\left|\frac{I_{Hn}}{I_{H1}}\right|^2 \tag{1}$$

where I_{Hn} is the nth harmonic component of the tank's current. The literature suggests that this shift is static but any fluctuation in I_{Hn}/I_{H1} due to the 1/f noise modulates $\Delta\omega$ and exhibits itself as 1/f^3 PN [11] [see Fig. 2(c)]. Although this mechanism has been known for quite some time, it is still not well understood how the flicker noise modifies the I_{Hn}/I_{H1} ratio. Furthermore, (1) suggests all harmonics *indiscriminately* modulate the Groszkowski's frequency shift by roughly the same amount, without regard to their odd/even-mode nature, which could be easily misinterpreted during the study of the flicker noise upconversion in cross-coupled oscillators.

While recognizing the Groszkowski's frequency shift as the dominant physical mechanism in voltage-biased oscillators, we turn our attention to the impulse sensitivity function (ISF) theory in researching the above-mentioned questions. Hajimiri and Lee [12] have shown that the upconversion of any flicker noise source depends on the dc value of the related effective ISF, which can be significantly reduced if the waveform has certain symmetry properties [12], [13]. Another explanation was offered in [14] and [15], suggesting that if the 1/f noise current of a switching MOS transistor is to be modeled by a product of stationary noise and a periodic function *w(t)*, then this noise can upconvert to PN if *w(t)* is asymmetric. In this paper, we elaborate on a method proposed in [23] to effectively trap the second current harmonic into a resistive path of a tank in a *voltage-biased* oscillator topology. Doing so will reduce the core transistors' low-frequency noise upconversion by making the oscillation waveform symmetric and reducing the effective ISF dc value. We further investigate the effects of harmonics on the core transistors' flicker noise upconversion by studying their impact on the oscillation waveform and on the effective ISF, $\Gamma_{\mathrm{eff,dc}}$.

It should be mentioned that several solutions are proposed in the literature to reduce the 1/f noise upconversion due to Groszkowski's frequency shift. The concept of a harmonically rich tank current degrading the close-in oscillator spectrum has been noticed for quite some time; however, the proposed solutions mostly include the linearization of the system to reduce the level of current harmonics by limiting the oscillation amplitude by an AGC [16], [17], or the linearization of gm-devices [18], [19], at the expense of the oscillator's start-up margin and increased 1/f^2 PN. In a completely different strategy, a resistor is added in [20] in series with gm-device drains. An optimum value of the resistor minimizes the flicker noise upconversion; however, the 1/f noise improvement is at the expense of the 20 dB/decade degradation in oscillators with low V_{DD} and high current consumption. The flicker noise upconversion due to nonlinearity of voltage-biased oscillators is quantified in detail in [21] and [22] and improved by limiting oscillator's excess gain [22].

This paper is organized as follows. Section II shows how harmonic components of the drain current contribute to the flicker noise upconversion and shows how an auxiliary common-mode (CM) resonance at $2\omega_0$ mitigates this upconversion. Section III demonstrates how the auxiliary resonance is realized and proves the effectiveness of the proposed method by implementing two classes of voltage-biased oscillators. Section IV reveals the details of circuit implementations and measurement results.

II. Method to Reduce 1/f Noise Upconversion

A. Auxiliary Resonant Frequencies

Let us start by focusing on reducing the Groszkowski frequency shift. As shown in Fig. 2(a)(c), the oscillation frequency ω_{osc} fluctuates around the tank's natural resonant frequency ω_0 due to the flow of higher harmonics of the current $I_{D1,2}$ into the capacitive part of the tank.

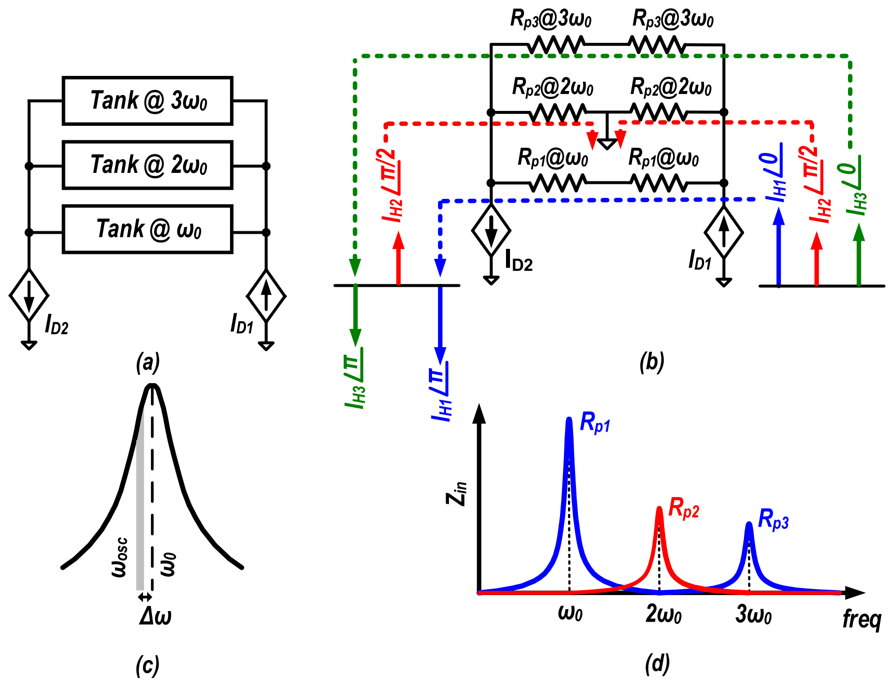

Fig. 3. Multiresonance tank. (a) Auxiliary resonances at higher harmonics. (b) Current harmonic paths. (c) Frequency drift due to higher harmonics. (d) Input impedances.

A voltage-biased class-B tank current in time and frequency domains is shown in Fig. 2(b). Odd harmonics of the tank current are differential-mode (DM) signals, and hence, they can flow into both differential- and single-ended (SE) capacitors. Even harmonics of the tank current, on the other hand, are CM signals, and can only flow into SE capacitors. If the tank possesses further resonances coinciding with these higher harmonics [see Fig. 3(a)], these components can find their respective resistive path to flow into, as shown in Fig. 3(b). Consequently, the capacitive reactive energy would not be disturbed and the oscillation frequency shift $\Delta\omega$ would be minimized [see Fig. 3(c)]. The input impedance Z_{in} of such a tank is shown in Fig. 3(d). The tank has the fundamental natural resonant frequency at ω_0 and auxiliary CM and DM resonant frequencies at even- and odd-order harmonics, respectively. Minimizing the frequency shift $\Delta\omega$ will weaken the underlying mechanism of the 1/f noise upconversion; however, realizing auxiliary resonances at higher harmonics has typically been area inefficient and can also degrade the PN performance. Consequently, the auxiliary resonance frequencies have to be chosen wisely.

Groszkowski frequency shift formula (1) indicates that all the contributing current harmonics I_{Hn} are weighted by almost the same coefficients. This means that, in practice, stronger current harmonics I_{Hn} contribute more to the frequency shift. Consequently, we can narrow down the required auxiliary resonances to these harmonics. On the other hand, ultimately, the low-frequency noise upconversion depends on the oscillation waveform and the dc value of effective ISF. The various current harmonics contribute unevenly to the flicker noise upconversion, since they result in different oscillation waveforms and effective ISF values. Investigating these differences reveals how many and at which frequencies the auxiliary resonances should be realized.

B. Harmonic Effects on the Effective ISF

A (hypothetical) sinusoidal resonance tank current $I_{H1}(t) = |I_{H1}|\sin(\omega_0 t)$ would result in a sinusoidal resonance oscillation voltage: $V_{H1}(t) = R_{p1}\cdot|I_{H1}|\sin(\omega_0 t) = A_1\sin(\omega_0 t)$. Its ISF is also a zero-mean sinusoid but in quadrature with $V_{H1}(t)$ [24]. The flicker noise of core transistors [e.g., $M_{1,2}$ in Fig. 4(a)] in a cross-coupled oscillator is modeled by a current source between the source and drain terminals, and exhibits a power spectral density as

$$\overline{i_n^2(t)} = \frac{K}{WLC_{ox}}\cdot\frac{1}{f}\cdot g_m^2(\omega_0 t) \tag{2}$$

where K is a process-dependent constant, W and L are core transistors' width and length, respectively, and C_{ox} is an oxide capacitance per area. Due to the dependence of current noise on g_m, the flicker noise source is a cyclostationary process and can be expressed as

$$i_n(t) = i_{n0}(\omega_0 t)\cdot\alpha(\omega_0 t) \tag{3}$$

in which $i_{n,0}(\omega_0 t)$ shows the stochastic stationarity. $\alpha(\omega_0 t)$ is the noise modulating function (NMF), which is normalized, deterministic, and periodic with the maximum of 1. It describes the noise amplitude modulation; consequently it should be derived from the cyclostationary noise characteristics [12]. In this case, an *effective* ISF is defined as $\Gamma_{eff}(\omega_0 t) = \alpha(\omega_0 t)\cdot\Gamma(\omega_0 t)$. $M_{1,2}$ flicker noise cannot upconvert to PN if effective ISF has a zero dc value.

Let us investigate the $M_{1,2}$ flicker noise upconversion when the oscillation voltage ideally contains only the

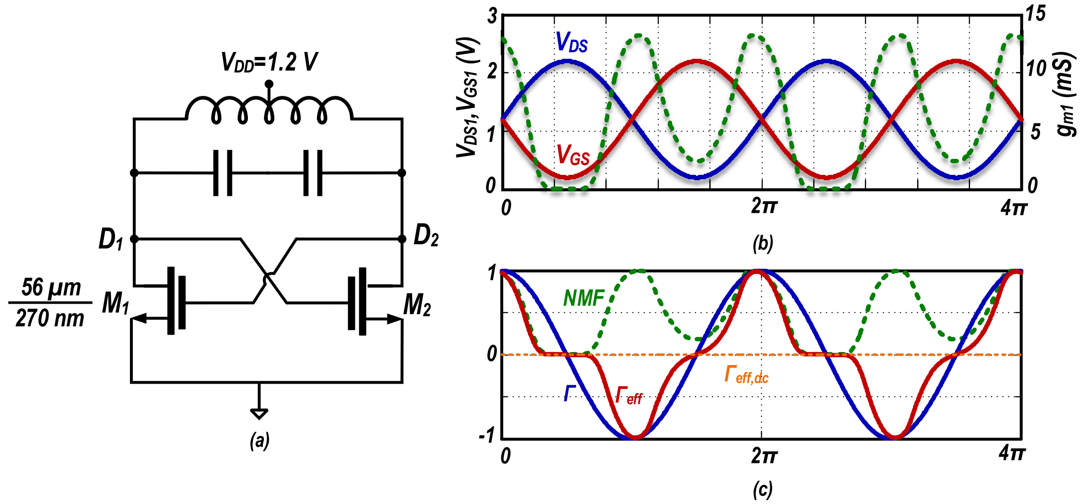

Fig. 4. Oscillator example. (a) Schematic and (b) V_{DS}, V_{GS}, and g_m of M_1 transistor when oscillation voltage contains only fundamental component and (c) its ISF, NMF, and effective ISF.

fundamental component. In Fig. 4(a), $V_{D1} = V_{DD} - A_1 \sin(\omega_0 t)$, $V_{G1} = V_{D2} = V_{DD} + A_1 \sin(\omega_0 t)$. Assuming $V_{DD} = 1.2$ V and $A_1 = 1$ V, g_m of the M_1 transistor under such V_{DS} and V_{GS} is found by simulations and is shown as dotted line in Fig. 4(b). Under this condition, $\alpha(\omega_0 t) = g_m(\omega_0 t)/g_{m,\max}$. ISF, NMF, and the effective ISF of the M_1 flicker noise source are shown in Fig. 4(c). The dc value of such an effective ISF is zero, resulting in no flicker noise upconversion. This is a well-known conclusion and is referred to as a state where $M_{1,2}$ transistors' flicker noise cannot upconvert to PN [15].

In reality, the tank current of voltage-biased oscillators is rich in harmonics. Due to physical circuit constraints, the even-order current harmonics lead by $\pi/2$, while the odd-order current harmonics are in-phase with the fundamental current I_{H1}. The $\pi/2$ phase difference in even- and odd-order current harmonics considerably changes the oscillation waveforms characteristics. For simplicity, we focus only on dominant harmonics, $I_{H2} = |I_{H2}| \sin(2\omega_0 t + \pi/2)$ and $I_{H3} = |I_{H3}| \sin(3\omega_0 t)$, as representatives of even- and odd-order current harmonics, respectively; however, the following discussion can be easily generalized for all harmonics. We also assume for now that the tank only contains SE capacitors.

The differential current I_{H2} flows into the SE capacitors and creates a second-order voltage harmonic

$$\begin{aligned} V_{H2}(t) &= \frac{1}{C \cdot 2\omega_0} \cdot |I_{H2}| \sin(2\omega_0 t + \pi/2 - \pi/2) \\ &= \alpha_2 A_1 \sin(2\omega_0 t) \end{aligned} \tag{4}$$

where the $-\pi/2$ phase shift is due to the capacitive load. The oscillation voltage will then be

$$\begin{aligned} V_{T2}(t) &= V_{H1}(t) + V_{H2}(t) \\ &= A_1[\sin(\omega_0 t) + \alpha_2 \sin(2\omega_0 t)]. \end{aligned} \tag{5}$$

$V_{H1}(t)$, $V_{H2}(t)$, and $V_{T2}(t)$ are plotted in Fig. 5(a) for $\alpha_2 = 0.1$ and $A_1 = 1$ V. $V_{H1}(t)$ has two zero crossings within its period: at t_1 and t_2, and their rise and fall times are symmetric with derivatives: $V'_{H1}(t_1) = -V'_{H1}(t_2)$. V_{H2}'s zero crossings are also at t_1 and t_2; however, $V'_{H2}(t_1) = V'_{H2}(t_2)$. Consequently, the opposite slope polarities of V_{H1} and V_{H2} at t_1 slow the fall time of V_{T2} while the same slope polarities at t_2 sharpen its rise time. Consequently, as can be gathered from 5(a), V_{T2} features *asymmetric* rise and fall slopes.

The resulting ISF of the g_m transistor is calculated based on (36) in [12] and is shown in Fig. 5(b), with its mean dependent on α_2. Larger α_2 leads to more asymmetry between $V_{T2}(t)$ rise and fall slopes; hence, $\Gamma_{\mathrm{eff,dc}}$ will increase. Furthermore, repeating the same simulations to obtain g_{m1} with drain and gate voltages that contain the second harmonic components results in asymmetric g_{m1} and consequently NMF. The slower rise/fall times increase the duration when M_1 is turned on, thus widening g_{m1}. A sharper rise/fall time decreases the amount of time when M_1 is turned on, resulting in a narrower g_{m1}. The NMF and effective ISF of such waveforms are shown in Fig. 5(b). The effective ISF has a dc value, which results in $M_{1,2}$'s flicker to PN upconversion. Dependence of the dc value of the effective ISF on α_2 is shown in Fig. 5(c).

This argument is valid for all even-order current harmonics, and we can conclude that the fluctuations in the even harmonics of the tank's current convert to the 1/f^3 PN noise through the modulation of the oscillating waveform.

Let us now investigate a case of the tank current containing only odd-harmonic components, with $I_{H3} = |I_{H3}| \sin(3\omega_0 t)$ as a representative. I_{H3} flows mainly into the tank capacitors and creates a third harmonic voltage as

$$\begin{aligned} V_{H3}(t) &= \frac{1}{C \cdot 3\omega_0} \cdot |I_{H3}| \sin(3\omega_0 t - \pi/2) \\ &= \alpha_3 A_1 \sin(3\omega_0 t - \pi/2) \end{aligned} \tag{6}$$

where again, the $-\pi/2$ phase shift is due to the capacitive load. The oscillation voltage will then be

$$\begin{aligned} V_{T3}(t) &= V_{H1}(t) + V_{H3}(t) \\ &= A_1[\sin(\omega_0 t) + \alpha_3 \sin(3\omega_0 t - \pi/2)]. \end{aligned} \tag{7}$$

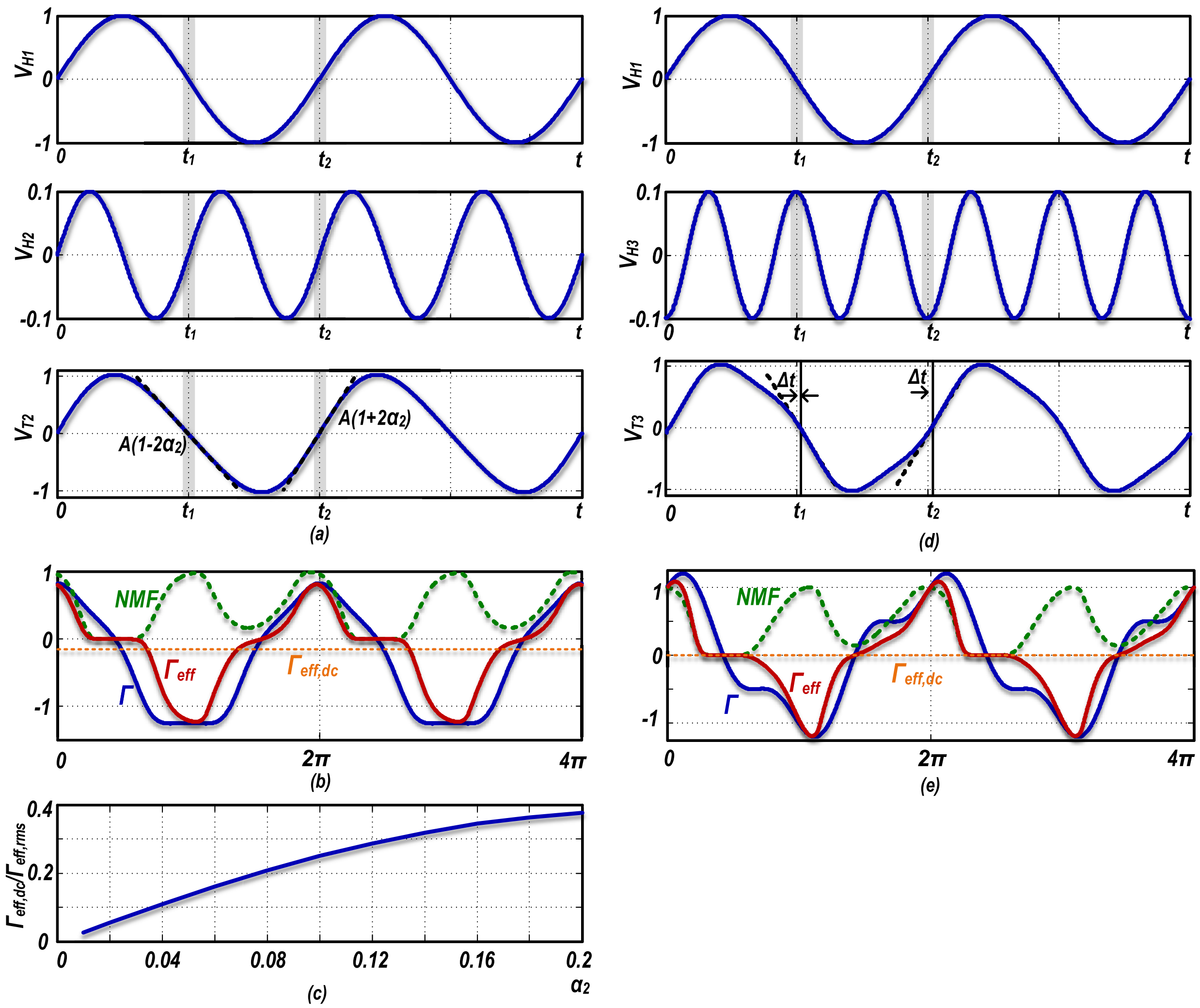

Fig. 5. Conventional tank waveforms. (a) Fundamental, V_{H1}, second harmonic, V_{H2}, voltage components, and oscillation waveform, V_{T2} and (b) its ISF, NMF, and effective ISF. (c) $\Gamma_{\text{eff,dc}}/\Gamma_{\text{eff,rms}}$ for different α_2 values. (d) Fundamental, V_{H1}, third harmonic, V_{H3}, voltage components, and oscillation waveform, V_{T3} and (e) its ISF, NMF, and effective ISF.

$V_{H1}(t)$, $V_{H3}(t)$, and $V_{T3}(t)$ are plotted in Fig. 5(d) for $\alpha_3 = 0.1$ and $A_1 = 1$ V. It is obvious that the oscillation waveform's falling and rising slopes are symmetric, and $\Gamma_{\text{dc}} = 0$, as easily gathered from Fig. 5(e). The simulations show that g_{m1} is slightly asymmetric due to amplitude distortion of the oscillation voltage. However, this asymmetry is canceled out when multiplied by ISF (see Fig. 5), resulting in an effective ISF with almost zero dc value and thus preventing low-frequency noise upconversion. These arguments can be generalized for all odd-order harmonics. Consequently, the low-frequency noise of g_m transistors does not upconvert to PN if the tank current only contains odd harmonics.

C. Resonant Frequency at $2\omega_0$

Thus far, we have shown that the even components of the tank's current are chiefly accountable for the asymmetric oscillation waveform and the 1/f noise upconversion to PN. Let us investigate what happens to the oscillation waveform and effective ISF if the tank has an auxiliary CM resonance at $2\omega_0$. Such resonance provides a resistive (i.e., via R_{p2}) path for I_{H2} to flow into it, and hence, the voltage second harmonic component is

$$\begin{aligned} V_{H2,\text{aux}}(t) &= R_{p2}|I_{H2}|\sin(2\omega_0 t + \pi/2) \\ &= A_1\alpha_{2,\text{aux}}\sin(2\omega_0 t + \pi/2). \end{aligned} \tag{8}$$

The composite oscillation voltage will become

$$\begin{aligned} V_{T2,\text{aux}}(t) &= V_{H1}(t) + V_{H2,\text{aux}}(t) \\ &= A_1[\sin(\omega_0 t) + \alpha_{2,\text{aux}}\sin(2\omega_0 t + \pi/2)]. \end{aligned} \tag{9}$$

$V_{H1}(t)$, $V_{H2,\text{aux}}(t)$, and $V_{T2,\text{aux}}(t)$ are plotted in Fig. 6(a)–(c) for $\alpha_{2,\text{aux}} = 0.1$ and $A_1 = 1$ V. The rise and fall times of the oscillation voltage are now symmetric [see Fig. 6(c)] and so the ISF is zero mean, as shown in Fig. 6(d). g_{m1}, and thus NMF, are also completely symmetrical; consequently, the effective ISF has a zero dc value, preventing low-frequency noise from being upconverted. The oscillation waveform is still dependent on $\alpha_{2,\text{aux}}$, but the rise and fall times are always symmetric, thus keeping $\Gamma_{\text{eff,dc}}$ zero.

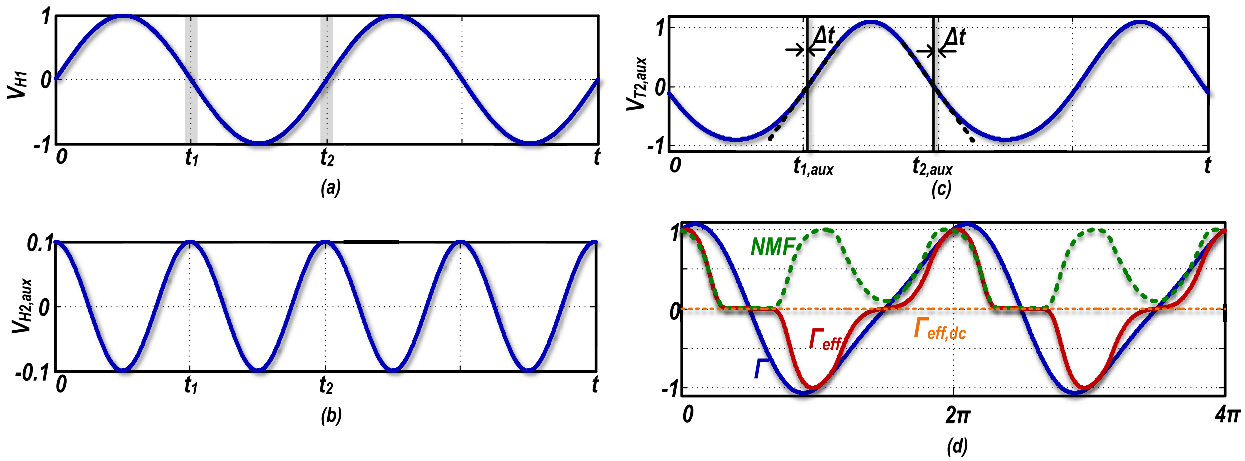

Fig. 6. Proposed tank waveforms. (a) Fundamental voltage component, V_{H1}, (b) voltage second harmonic in the presence of auxiliary resonance, $V_{H2,\text{aux}}$, (c) oscillation waveform, $V_{T2,\text{aux}}$, and (d) its ISF, NMF, and effective ISF.

The second and third current harmonics are the most dominant in all classes of oscillators, so α_2 and α_3 are significantly larger than other α_n for $n = 4, 5, \ldots$. Meanwhile, Γ_{dc} is a growing function of α_n for $n = 2k$, where $k = 1, 2, \ldots$. We can, therefore, conclude that I_{H2} is the main contributor to the 1/f noise upconversion. Consequently, attention to only one auxiliary resonant frequency at $2\omega_0$ appears sufficient [23], [25].

D. ω_{CM} Deviation From $2\omega_0$

The balance in the rise and fall zero-crossing slopes in Fig. 6(c) is rooted in the $\pi/2$ phase shift between $V_{H1}(t)$ and $V_{H2}(t)$. This is a combination of the $\pi/2$ phase difference between $I_{H1}(t)$ and $I_{H2}(t)$, and zero phase of the resistive tank impedance at $2\omega_0$. When ω_{CM} deviates from $2\omega_0$

$$\begin{aligned} V_{T2,\text{aux}}(t) &= V_{H1}(t) + V_{H2,\text{aux}}(t) \\ &= R_{p1}|I_{H1}|\sin(\omega_0 t) + |Z_{\text{CM}}| \\ &\quad \cdot |I_{H2}|\sin(2\omega_0 t + \pi/2 + \phi_{\text{CM}}) \\ &= A_1[\sin(\omega_0 t) + \alpha_{2,\text{aux}}\sin(2\omega_0 t + \pi/2 + \phi_{\text{CM}})] \end{aligned} \tag{10}$$

where $|Z_{\text{CM}}|$ and ϕ_{CM} are the CM input impedance magnitude and phase, respectively, derived as

$$\phi_{\text{CM}} = \arctan\left(\frac{1-\zeta^2}{\frac{\zeta}{Q_{\text{CM}}}}\right) \tag{11}$$

$$|Z_{\text{CM}}| = R_{p2} \cdot \frac{\frac{\zeta}{Q_{\text{CM}}}}{\sqrt{(1-\zeta^2)^2 + \left(\frac{\zeta}{Q_{\text{CM}}}\right)^2}} \tag{12}$$

where $\zeta = 2\omega_0/\omega_{\text{CM}}$. ω_{CM} versus $2\omega_0$ misalignment has two effects. The first directly translates ϕ_{CM} into the waveform asymmetry. Fig. 7(a) shows $V_{T2,\text{aux}}(t)$ for different ϕ_{CM} values; $\alpha_{2,\text{aux}}$ was chosen 0.3 to better illustrate the asymmetry. When grossly mistuned from $2\omega_0$, ϕ_{CM} could approach $\pm\pi/2$, thus making the auxiliary resonance completely ineffective. A larger Q-factor of the CM resonance, Q_{CM}, results in ϕ_{CM} closer to $\pm\pi/2$ for the same $2\omega_0/\omega_{\text{CM}}$ ratios, as shown in Fig. 7(b).

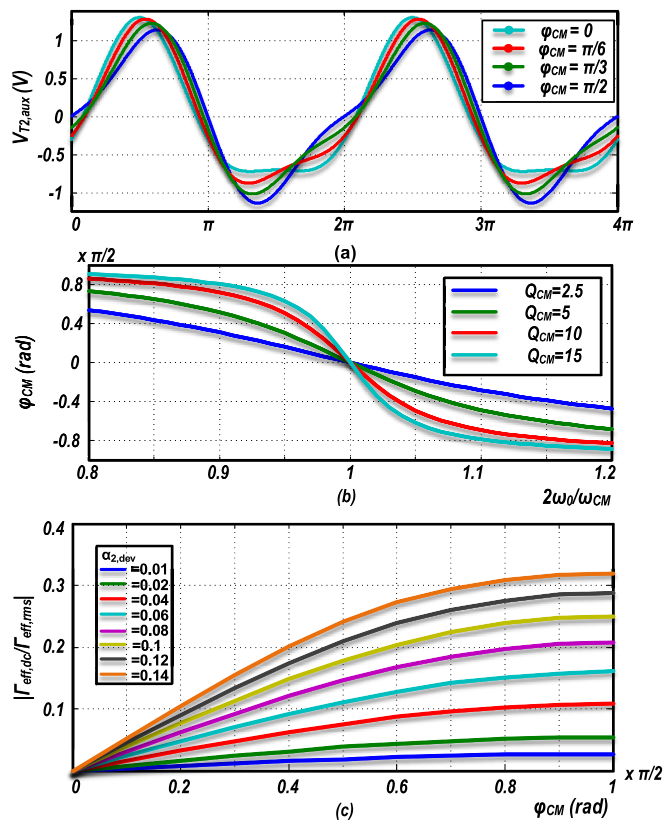

Fig. 7. (a) $V_{T2,\text{aux}}$ for different ϕ_{CM} values. (b) ϕ_{CM} for different Q_{CM} values when ω_{CM} deviates from $2\omega_0$. (c) $\Gamma_{\text{eff,dc}}/\Gamma_{\text{eff,rms}}$ for different $\alpha_{2,\text{aux}}$ and ϕ_{CM} values.

The second effect is due to $\alpha_{2,\text{aux}}$, which determines the amount of the second harmonic in the voltage waveform. When ϕ_{CM} is not zero, $\Gamma_{\text{eff,dc}}$ becomes dependent on $\alpha_{2,\text{aux}}$: the larger $\alpha_{2,\text{aux}}$, the more asymmetric waveform, and more 1/f noise upconversion. The $\alpha_{2,\text{aux}}$ value can be found from the following equation:

$$\alpha_{2,\text{aux}} = \left|\frac{I_{H2}}{I_{H1}}\right| \cdot \frac{|Z_{\text{CM}}|}{R_{p1}}. \tag{13}$$

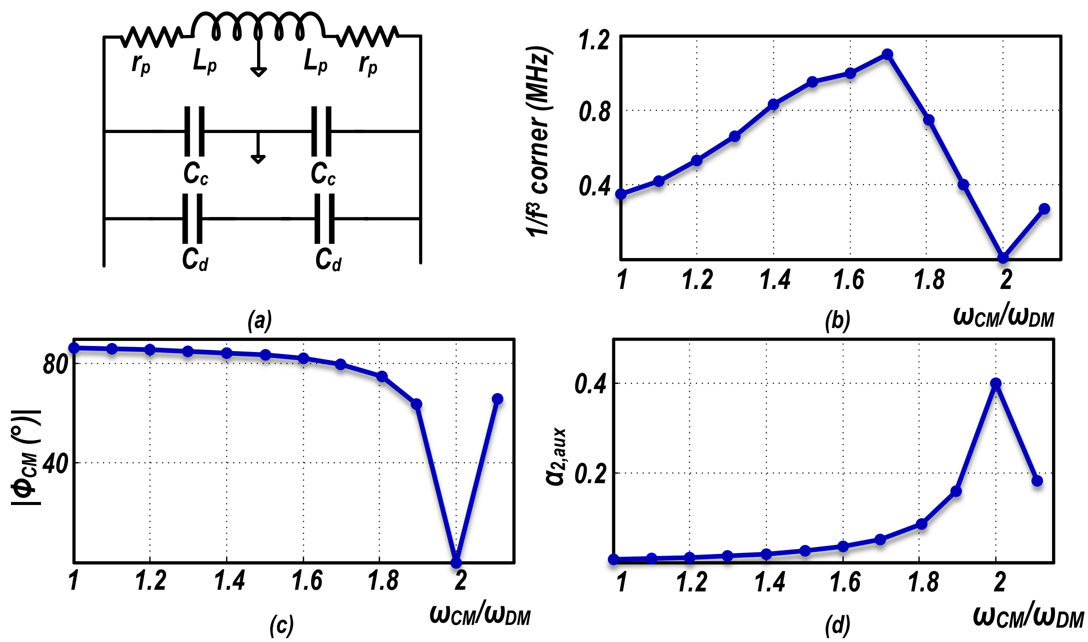

Fig. 8. (a) Tank with DM and CM resonances, (b) 1/f^3 corner of the oscillator employing this tank, (c) ϕ_{CM}, and (d) $\alpha_{2,\mathrm{aux}}$ of the tank versus $\omega_{\mathrm{CM}}/\omega_{\mathrm{DM}}$.

I_{H2}/I_{H1} is dependent on the oscillator's topology. Furthermore, the larger the Q_{CM} value, the larger the R_{p2} value and, hence, the larger the $\alpha_{2,\mathrm{aux}}$ value. Fig. 7(c) shows the expected $\Gamma_{\mathrm{eff,dc}}/\Gamma_{\mathrm{eff,rms}}$ versus ϕ_{CM} for different $\alpha_{2,\mathrm{aux}}$ values. Both of these effects point out that Q_{CM} should be low to reduce the sensitivity of this method to the ω_{CM} deviation from $2\omega_0$.

III. Circuit Implementation

We have shown that if the tank demonstrates an auxiliary CM resonance at the second harmonic of its fundamental ω_0 resonance, the oscillation waveform would be symmetric, and hence, the flicker noise upconversion would be suppressed. Since the differential capacitors are not seen by the CM signals (i.e., I_{H2}), a straightforward solution for realizing a CM peak is to design a tank, as demonstrated in Fig. 8(a) with a set of differential C_d and SE C_c capacitors [25]. r_p is the equivalent series resistance of the inductor and it is assumed all capacitors are nearly ideal. This tank shows a fundamental DM resonant frequency, $\omega_{DM} = \frac{1}{\sqrt{L_p(C_c+C_d)}}$ and a CM resonant frequency $\omega_{CM} = \frac{1}{\sqrt{L_pC_c}}$. From (11)–(13)

$$\phi_{\mathrm{CM}} = \arctan\left(\frac{1-\frac{4C_c}{C_c+C_d}}{\frac{1}{Q_{\mathrm{DM}}}\cdot\frac{2C_c}{C_c+C_d}}\right) \quad (14)$$

$$\alpha_{2,\mathrm{aux}} = \frac{R_{p2}}{R_{p1}}\cdot\frac{\frac{2}{Q_{\mathrm{DM}}}\cdot\left(\frac{C_c}{C_c+C_d}\right)}{\sqrt{\left(1-\frac{4C_c}{C_c+C_d}\right)^2+\left(\frac{2}{Q_{\mathrm{DM}}}\cdot\frac{C_c}{C_c+C_d}\right)^2}}\cdot\frac{I_{H2}}{I_{H1}} \quad (15)$$

where Q_{DM}, R_{p2}, and R_{p1} are, respectively, the quality factor at DM resonance, and impedance peaks at CM and DM resonances. In an extreme condition of $C_d = 0$, the tank contains only the SE capacitors and reduces to a conventional tank discussed in Section II-B. Targeting $\omega_{\mathrm{CM}} = 2\omega_{\mathrm{DM}}$ results in $C_d = 3C_c$ and we can prove that $Q_{\mathrm{CM}} = 2Q_{\mathrm{DM}}$. As discussed supra, the fairly large Q_{CM} exacerbates the effects of CM resonance misalignment.

To investigate the effectiveness of the proposed method on the tank mistuning sensitivity, we performed an analysis of a 5 GHz voltage-biased class-B oscillator of Fig. 1(b) with $Q_{\mathrm{DM}} = 10$. The oscillator is designed in a 40 nm CMOS technology, and $M_{1,2}$ values are thick-oxide (56/0.27) μm devices. The power consumption is 10.8 mW at $V_{DD} = 1.2$ V. As expected, the 1/f^3 corner of this oscillator is at its minimum of ~10 kHz at $C_d/C_c = 3$ [see Fig. 8(b)]. When ω_{CM} deviates from $2\omega_{\mathrm{DM}}$, i.e., C_d/C_c ratio deviates from the ideal value of 3, while keeping $C_c + C_d$ constant, the 1/f^3 corner starts to increase from the 10 kHz minimum, and reaches its peak at $\omega_{\mathrm{CM}} = 1.7\omega_{\mathrm{DM}}$ when the CM resonance phase, ϕ_{CM}, gets close to $\pi/2$ [about 80° as shown in Fig. 8(c)]. After this point, the ϕ_{CM} value barely changes, but $\alpha_{2,\mathrm{aux}}$ decreases [Fig. 8(d)], and consequently, the 1/f^3 corner reduces again. The maximum 1/f^3 corner of 1.1 MHz is actually much worse than the 400 kHz corner of extreme case when $C_d = 0$ [see Fig. 8(b)]. This means that if the tank is not designed properly, the performance would be even worse than that without applying this technique. Consequently, to ensure no performance degradation in face of the misalignment, $\alpha_{2,\mathrm{aux}}$ at $\phi_{\mathrm{CM}} \approx 80°$ should be less than that of the tank without the applied technique. α_2, when $C_d = 0$, can be found from (15)

$$\alpha_2 \approx \frac{2}{3Q_{\mathrm{DM}}}\cdot\frac{I_{H2}}{I_{H1}} \quad (16)$$

$\phi_{\mathrm{CM}} = 80°$, (14) and (15) result in

$$\alpha_{2,\mathrm{aux}} = \frac{R_{p2}}{R_{p1}}\cdot\frac{\tan\left(\frac{\pi}{18}\right)}{\sqrt{1+\tan^2\left(\frac{\pi}{18}\right)}}\cdot\frac{I_{H2}}{I_{H1}}. \quad (17)$$

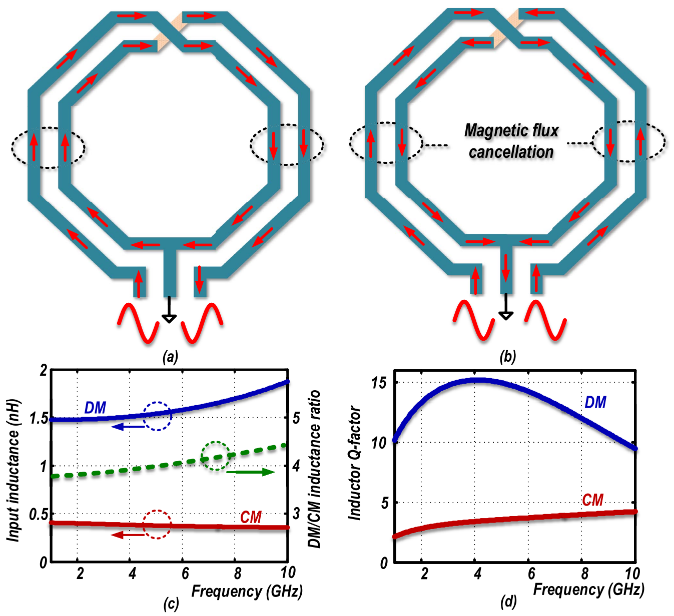

Fig. 9. Two-turn "F_2" inductor in (a) DM excitation, (b) CM excitation, (c) F_2 DM and CM inductances and their ratio, and (d) Q_{DM} and Q_{CM}.

Hence

$$\frac{R_{p2}}{R_{p1}} < \frac{3.84}{Q_{\mathrm{DM}}} \tag{18}$$

to satisfy this condition, which results in nonpractical Q_{DM} values.

In Sections III-A and III-B, we show how to substantially reduce the sensitivity to such misalignment by employing, at no extra area penalty, an inductor exhibiting distinct and beneficial characteristics in DM and CM excitations. The different behaviors of a 1:2 turn transformer in DM and CM excitations are also exploited to design a transformer-based F_2 tank. With these new tanks, we construct class-D and class-F oscillators to demonstrate the effectiveness of the proposed method of reducing the flicker noise upconversion.

A. Inductor-Based F_2 Tank

Fig. 9(a) and (b) shows a two-turn "F_2" inductor when it is excited by DM and CM signals. In the DM excitation, currents in both turns have the same direction, resulting in an additive magnetic flux. However, in the CM excitation, currents have opposite direction and cancel each other's flux [26]. With the proper spacing between the F_2 inductor windings, effective inductance in CM can be made four times smaller than in DM. The $L_{\mathrm{DM}}/L_{\mathrm{CM}}$ inductance ratio is controlled through lithography that *precisely* sets the physical inductor dimensions and, consequently, makes it *insensitive* to process variations. Fig. 9(c) shows the DM and CM inductances and their ratio over frequency. $L_{\mathrm{DM}}/L_{\mathrm{CM}}$ is close to 4 within a 30%–40% tuning range.

Differential capacitors cannot be seen by the CM signals; hence, to be able to set the CM resonance, the F_2 tank capacitors should be SE, as shown in Fig. 10(a). The F_2 tank demonstrates two resonant frequencies: ω_{DM} and ω_{CM}.

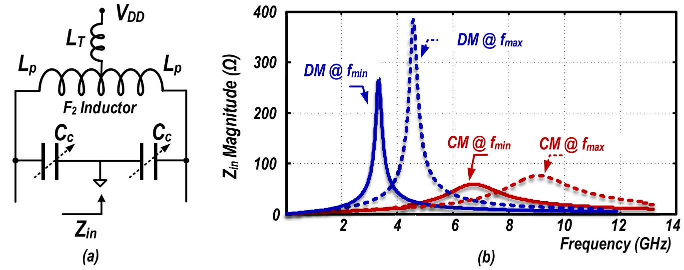

Fig. 10. (a) Inductor-based F_2 tank and (b) its input impedance.

Both of these are tuned simultaneously by adjusting C_c. The precise inductor geometry maintains $L_{\mathrm{DM}}/L_{\mathrm{CM}} \approx 4$ and, hence, $\omega_{\mathrm{CM}}/\omega_{\mathrm{DM}} \approx 2$ over the full tuning range.

The input impedance of the tank is shown in Fig. 10(b). Presuming that the capacitance losses are negligible, the DM and CM resonance quality factors are

$$Q_{\mathrm{DM}} = \frac{L_p \omega_{\mathrm{DM}}}{r_p} = Q_0 \tag{19}$$

$$Q_{\mathrm{CM}} = \frac{L_p \omega_{\mathrm{CM}}}{4 r_p} = \frac{Q_0}{2}. \tag{20}$$

The Q-factor of the CM resonance is half that of DM, which relaxes the F_2 tank sensitivity to mismatch between ω_{CM} and $2\omega_{\mathrm{DM}}$. For this inductor-based F_2 tank, $R_{p2}/R_{p1} = 0.25$, and the condition in (18) is *satisfied* for $Q_0 < 15$. Furthermore, in the CM excitation, the currents in adjacent windings have opposite direction, which results in an increased ac resistance [27], and so the Q-factor of the CM inductance is even smaller than in (20). The Q-factor of L_{CM} inductance of Fig. 9(b) is about 3–4.

Apart from the easy tuning with only one capacitor bank, the mostly SE parasitic capacitors do not play any role in defining the $\omega_{\mathrm{CM}}/2\omega_{\mathrm{DM}}$ ratio. Furthermore, the low Q_{CM} and, consequently, the lower sensitivity to the $\omega_{\mathrm{CM}}/2\omega_{\mathrm{DM}}$ ratio that the inductor-based F_2 tank offers make it all more attractive than the tank shown in Fig. 8(a).

B. Class-D/F_2 Oscillator

Among the various classes of inductor-based oscillators (e.g., class-B, complementary class-B, and class-D [4]), we have decided to validate the proposed method on a class-D oscillator shown in Fig. 11(a). This recently introduced oscillator shows promising PN performance in the $1/f^2$ region due its special ISF. The tail current transistor is removed there and wide and almost ideal switches $M_{1,2}$ clip the oscillation voltage to GND for half a period [see Fig. 11(b)] resulting in an almost zero ISF there [Fig. 11(c)]. However, the hard clipping of the drain nodes to GND generates a huge amount of higher order harmonic currents. Due to the large I_{H2}, in agreement with our analysis, the oscillating waveform has asymmetric fall and rise times [clearly visible in Fig. 11(b)], and it exhibits a strong 1/f noise upconversion and frequency pushing. A version of class-D with a tail filter technique [30] was also designed in [4] in an attempt to reduce the low-frequency noise upconversion. This method is partially

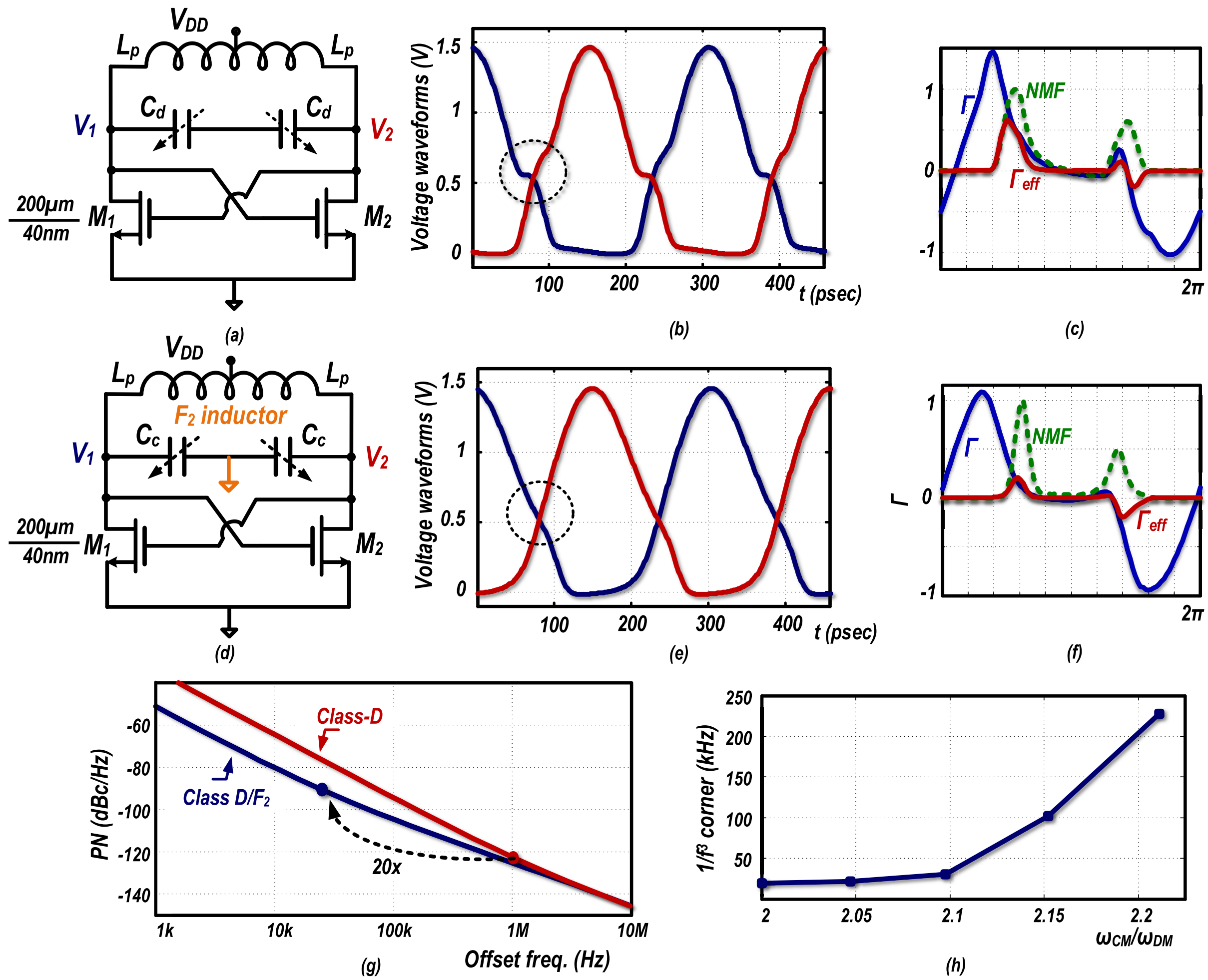

Fig. 11. Class-D oscillator. (a) Schematic and (b) its waveforms. (c) gm-transistor ISF, NMF, and effective ISF. Class-D/F$_2$ oscillator. (d) Schematic and (e) its waveforms. (f) gm-transistor ISF, NMF, and effective ISF and (g) their PN performance. (h) 1/f^3 corner sensitivity to $\omega_{\mathrm{CM}}/\omega_{\mathrm{DM}}$.

effective, lowering the 1/f^3 PN corner from 2 to 0.6–1 MHz. Due to the above-mentioned reasons, this voltage-biased oscillator seems a perfect fit for the proposed method.

Fig. 11(d) shows the proposed class-D/F$_2$ oscillator, which adopts the F_2 tank. The gm-devices, M_1 and M_2, still inject a large I_{H2} current into the tank, but this current is now flowing into the equivalent resistance of the tank at $2\omega_0$. Clearly, the rise/fall times are more symmetric in the class-D/F$_2$ oscillator, as demonstrated in Fig. 11(e). The gm-transistors' ISF, NMF, and effective ISF are shown in Fig. 11(f). As predicted, effective Γ_{dc} is now reduced, and the simulated PN performance shows that the 1/f^3 corner is lowered from 1 MHz to ∼30 kHz [Fig. 11(g)].

The parasitic inductance L_T [see Fig. 10(a)] has to be considered in designing the F$_2$ inductor. C_c controls both CM and DM resonant frequencies simultaneously; hence, any deviation of ω_{CM} from $2\omega_0$ is due to $L_{\mathrm{CM}}/L_{\mathrm{DM}}$ not being exactly 4 over the TR. To examine the robustness of the tank via simulations, a C_d differential capacitor is deliberately added to the tank. $C_c + C_d$ is kept constant in order to maintain the oscillation frequency. Doing so shifts up ω_{CM} while keeping ω_{DM} intact. Fig. 11(h) shows how the 1/f^3 corner worsens when C_d/C_c ratio increases.

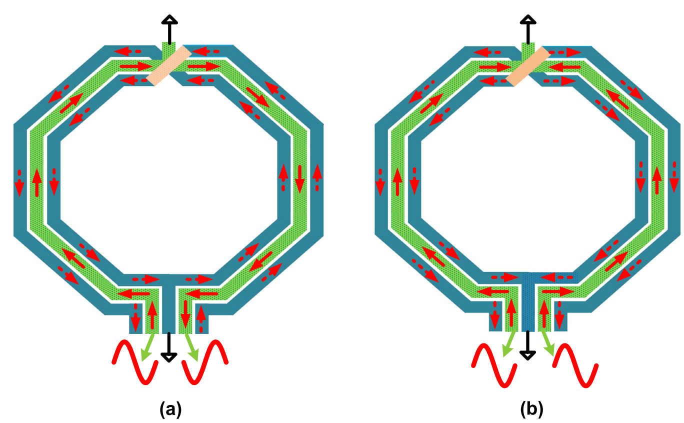

Fig. 12. 1:2 transformer when the primary is excited with (a) DM and (b) CM currents.

C. Transformer-Based F_2 Tank

Fig. 12(a) and (b) shows a 1:2 turns transformer excited by DM and CM input signals at its primary. With a DM excitation, the induced currents at the secondary circulate in the same direction leading to a strong coupling factor, k_m. On the other hand, in CM excitation, the induced currents

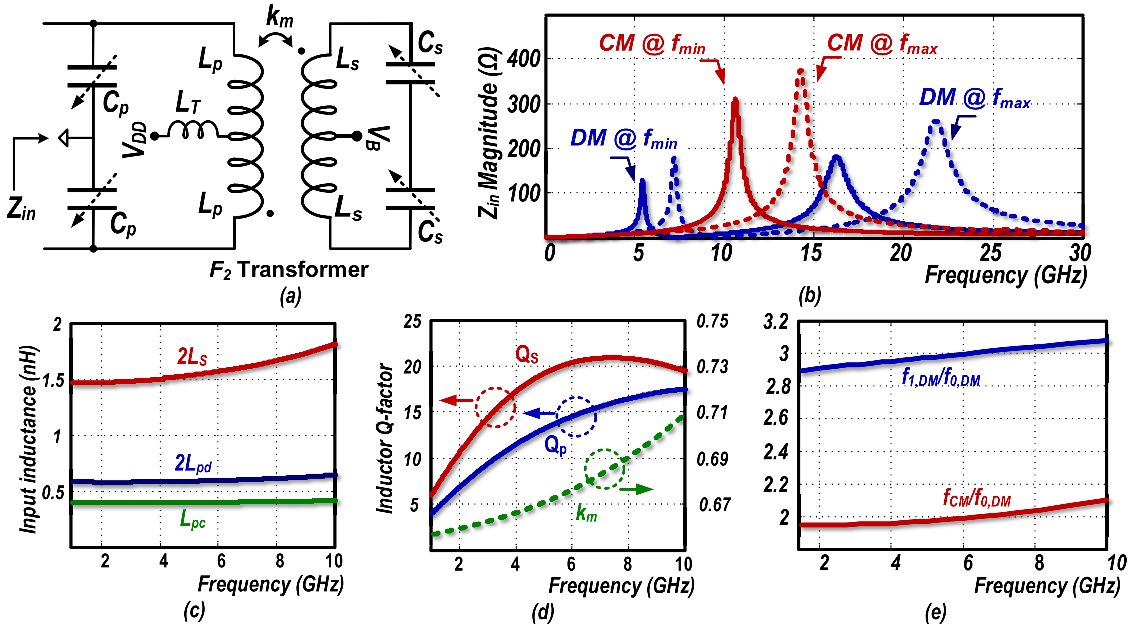

Fig. 13. (a) Transformer-based F_2 tank and (b) its input impedance. (c) DM and CM primary and secondary inductance. (d) Primary and secondary inductance quality factor and coupling factor. (e) DM and CM resonant frequencies over TR.

cancel each other, resulting in a weak k_m [28]. The latter means that the secondary winding cannot be seen by the CM signals. "F_2" transformer-based tank is shown in Fig. 13(a).

At the DM excitation, no current flows into the metal track inductance, L_T, that connects the center tap to the supply's ac-ground [see Fig. 13(a)]. However, at the CM excitation, the current flowing into L_T is twice the current circulating in the inductors. Consequently, the tank inductance L_p in Fig. 13(a) is relabeled as $L_{p,d} = L_p$ in DM, and $L_{p,c} = L_{p,d} + 2L_T$ in CM excitations. This tank employs SE primary and differential secondary capacitors and demonstrates two DM and one CM resonant frequencies. $\omega_{CM} = 1/\sqrt{L_{p,c}C_p}$, and if $k_{m,DM}>0.5$, $\omega_{0,DM} = 1/\sqrt{L_{p,d}C_p + L_s C_s}$ [5]. F_2 tank requires $\omega_{\mathrm{CM}} = 2\omega_{0,\mathrm{DM}}$, and hence

$$L_s C_s = C_p(4L_{p,c} - L_{p,d}). \tag{21}$$

Unlike in the inductor-based tank, here, the $\omega_{\mathrm{CM}}/\omega_{0,\mathrm{DM}}$ ratio is dependent on the secondary-to-primary capacitors ratio. Furthermore, the input impedance Z_{in}, shown in Fig. 13(b), reveals that Q_{CM} is not low, thus making it sensitive to $\omega_{\mathrm{CM}}/\omega_{0,\mathrm{DM}}$. It means that the C_s/C_p ratio has to be carefully designed to maintain $\omega_{\mathrm{CM}}/\omega_{0,\mathrm{DM}} \approx 2$ over the tuning range. In practice, the Q-factor of capacitor banks is finite and decreases at higher frequencies, so Q_{CM} will reduce, thus making the tank a bit less sensitive.

D. Class-$F_{2,3}$ Oscillator

As proved in [5], a DM auxiliary resonance at the third harmonic of the fundamental frequency is beneficial in improving the 20 dB/decade PN performance by creating a pseudo square-wave waveform (see Fig. 14). We can merge our transformer-based F_2 tank with the class-F_3 operation in [5] [see Fig. 14(a) and (b)] to design a class-$F_{2,3}$ oscillator, as shown in Fig. 14(d) and (e). To ensure $\omega_{\mathrm{CM}} = 2\omega_{0,\mathrm{DM}}$ and $\omega_{1,\mathrm{DM}} = 3\omega_{0,\mathrm{DM}}$, we force $L_s C_s = 3.8L_{p,d}C_p$ and $k_m = 0.67$. The relatively low k_m increases the impedance at $\omega_{1,\mathrm{DM}} \equiv 3\omega_{0,\mathrm{DM}}$ [29]. However, the class-F_3 oscillator meets the oscillation criteria only at $\omega_{0,\mathrm{DM}}$. Fig. 14(e) demonstrates that the pseudo-square waveform of class-F_3 oscillation is preserved in the class-$F_{2,3}$ oscillator. The waveform does not appear to differ much; however, the oscillation voltage spectrum indeed confirms the class-$F_{2,3}$ operation. I_{H2} is not very large in this class of oscillators; consequently, the fall/rise-time asymmetry is not as distinct as in the class-D oscillator. However, the 1/f^3 corner improvement from 400 kHz in class-F_3 to <30 kHz in class-$F_{2,3}$, as demonstrated in Fig. 14(g), proves the effectiveness of the method. The ISF, NMF, and effective ISFs for these oscillators are shown in Fig. 14(c) and (f).

Class-$F_{2,3}$ oscillator performance is sensitive to the deviation of ω_{CM} from $2\omega_0 \equiv 2\omega_{\mathrm{DM}}$. C_p changes both CM and DM resonant frequencies while C_s only changes the DM one. To examine the robustness of the F_2 operation, differential capacitors are added in the tank's primary. Here, again $C_{p,c} + C_{p,d}$ is constant to maintain the oscillation frequency. Fig. 14(h) shows the 1/f^3 corner versus $\omega_{\mathrm{CM}}/\omega_{\mathrm{DM}}$ ratio and underscores the need to control the capacitance ratio, as per (21). Otherwise, a small deviation increases the 1/f^3 corner rapidly, and with larger deviations, the method becomes ineffective.

IV. Experimental Results

The class-D/F_2 and class-$F_{2,3}$ oscillators, whose schematics were shown in Figs. 11(d) and 14(d), respectively, are designed in 40 nm CMOS to demonstrate the suppression of the 1/f noise upconversion. For fair comparison, we attempted to design the oscillators with the same specifications, such as center frequency, tuning range, and supply voltage, as their original reference designs in [4] and [5].

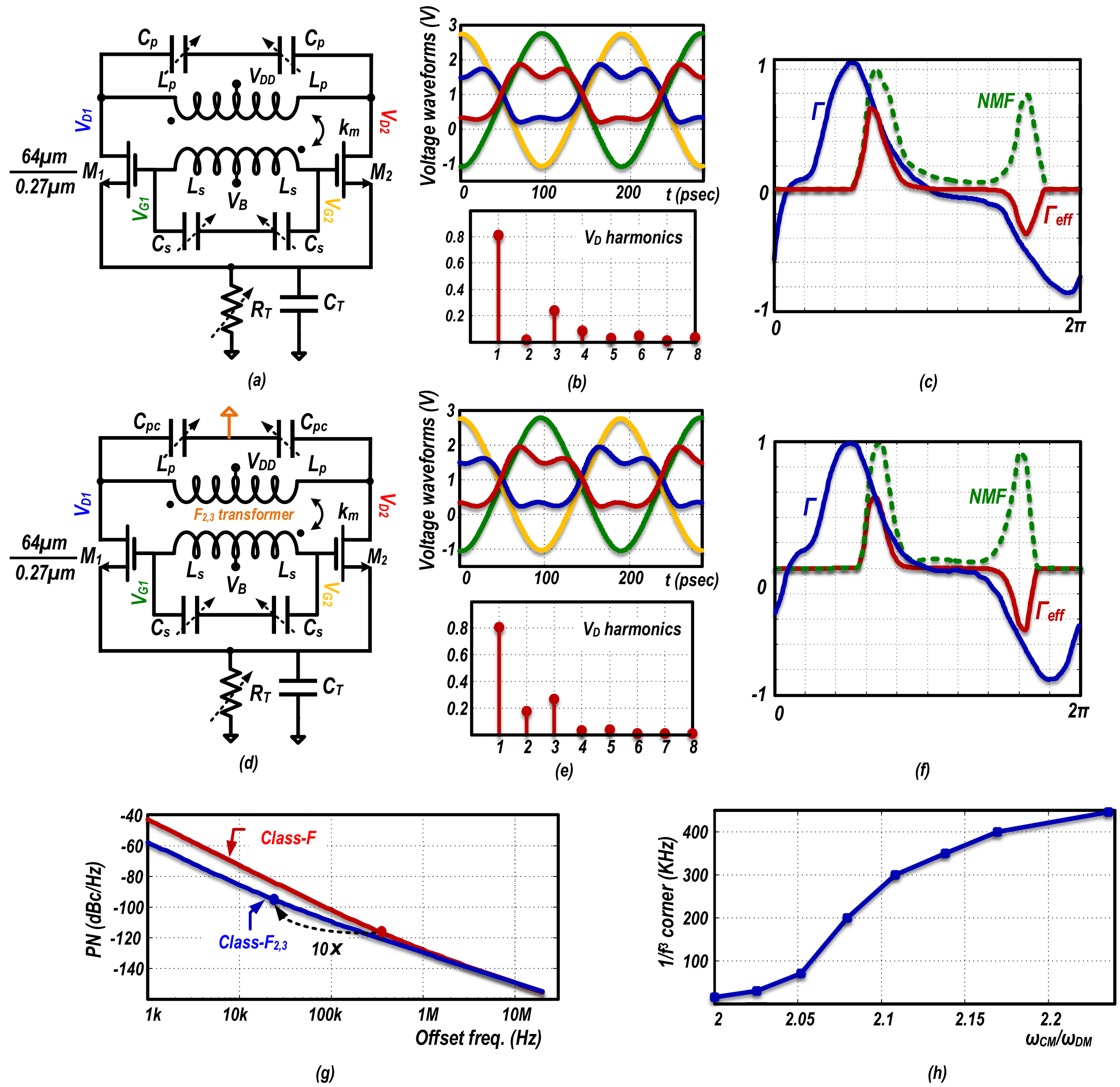

Fig. 14. Class-F$_3$ oscillator. (a) Schematic and (b) its waveforms with harmonic content. (c) gm-transistor ISF, NMF, and effective ISF. Class-F$_{2,3}$ oscillator. (d) Schematic and (e) its waveforms with harmonic content. (f) gm-transistor ISF, NMF, and effective ISF and (g) their PN performance. (h) 1/f^3 corner sensitivity to $\omega_{\mathrm{CM}}/\omega_{\mathrm{DM}}$.

A. Class-D/F$_2$ Oscillator

The class-D/F$_2$ oscillator is realized in a 40 nm 1P8M CMOS process *without* ultrathick metal layers. The two-turn inductor is constructed by stacking the 1.45 μm Alucap layer on top of the 0.85 μm top (M8 layer) copper metal. The DM inductance is 1.5 nH with the simulated Q of 12 at 3 GHz. Combination of MOS/MOM capacitors between the supply and the ground is placed on-chip to minimize the effective L_T inductance, and the remaining uncompensated inductance is modeled very carefully. The capacitor bank is realized with 6-b switchable MOM capacitors with the LSB of 30 fF. The oscillator is tunable between 3.3 and 4.5 GHz (31% TR) via this capacitor bank. $M_{1,2}$ transistors are (200/0.04) μm low-V$_t$ devices to ensure start-up and class-D operation over PVT. The chip micrograph is shown in Fig. 15(a) with a core area of 0.1 mm^2.

Fig. 16(a) shows the measured PN at $f_{\max}$ and $f_{\min}$ with V_{DD} = 0.5 V. Current consumption is 6 and 4 mA. The 1/f^3 corner is 100 kHz at $f_{\max}$ and reduces to 60 kHz for $f_{\min}$. The 1/f^3 corner over TR is shown in Fig. 16(c). The supply frequency pushing is 60 and 40 MHz/V at $f_{\max}$ and $f_{\min}$, respectively [see Fig. 16(b)]. Table I compares its performance with the original class-D oscillators (as well as other state-of-the-art oscillators [20], [25], [31] aimed at reducing the 1/f noise upconversion). Compared with the original design, the FoM at 10 MHz offset is degraded in the class-D/F$_2$ oscillator by 3 dB, mainly due to the lack of ultrathick metal layers, which lowers the inductor's Q. However, even with this degradation, FoM at 100 kHz offset is improved at least 3 dB. 1/f^3 corner is improved at least ten times versus both class-D and noise-filtering class-D oscillators.

B. Class-F$_{2,3}$ Oscillator

The class-F$_{2,3}$ oscillator is realized in 40 nm 1P7 CMOS process with ultrathick metal layer. The 1:2 transformer is constructed with the 3.4 μm top ultrathick (M7 layer)

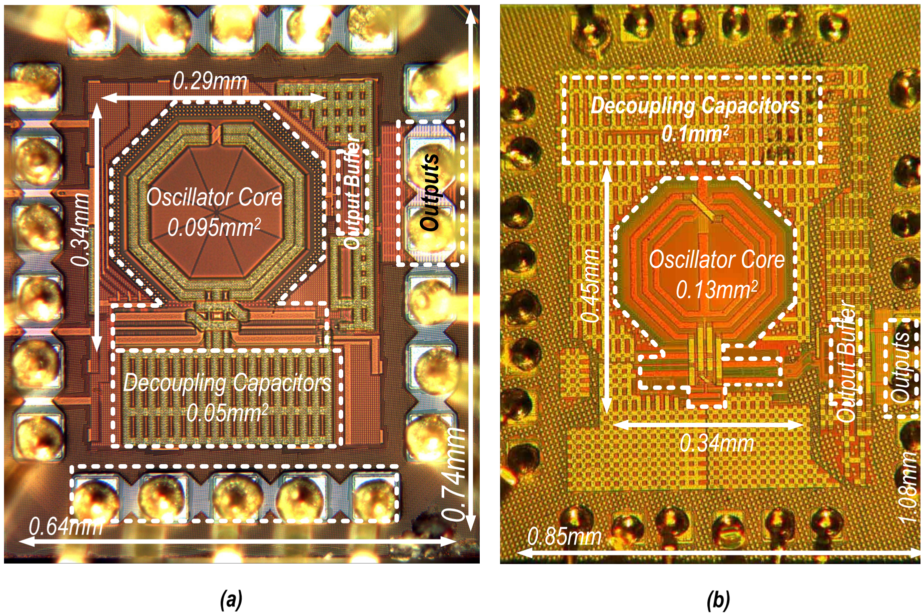

Fig. 15. Chip micrographs. (a) Class-D/F$_2$ oscillator. (b) Class-F$_{2,3}$ oscillator.

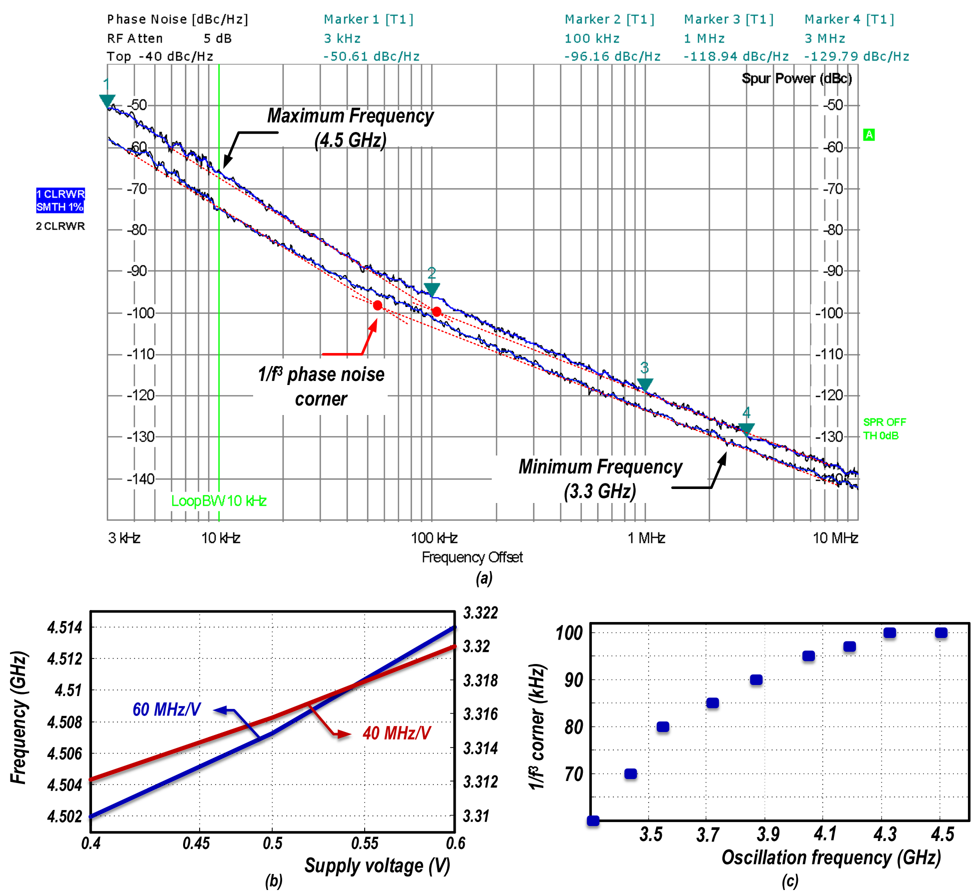

Fig. 16. Class-D/F$_2$ oscillator: measured (a) PN at $f_{\max}$ and $f_{\min}$, (b) frequency pushing due to supply voltage variation, and (c) 1/f^3 corner over tuning range.

copper metal. The primary and secondary winding inductances are 0.58 and 1.5 nH, respectively, and $k_m = 0.67$. The simulated Q-factors of the primary and secondary windings are 15 and 20 at 6 GHz. Like the class-D/F$_2$, the L_T inductance has to be compensated with enough decoupling capacitance. The unfiltered part has to be modeled precisely due to the relatively large R_{p2}. The SE primary and differential secondary capacitor banks are realized with two 6-b switchable MOM capacitors, with the LSB of 32 and 48 fF, respectively. Due to the sensitivity of this oscillator to the

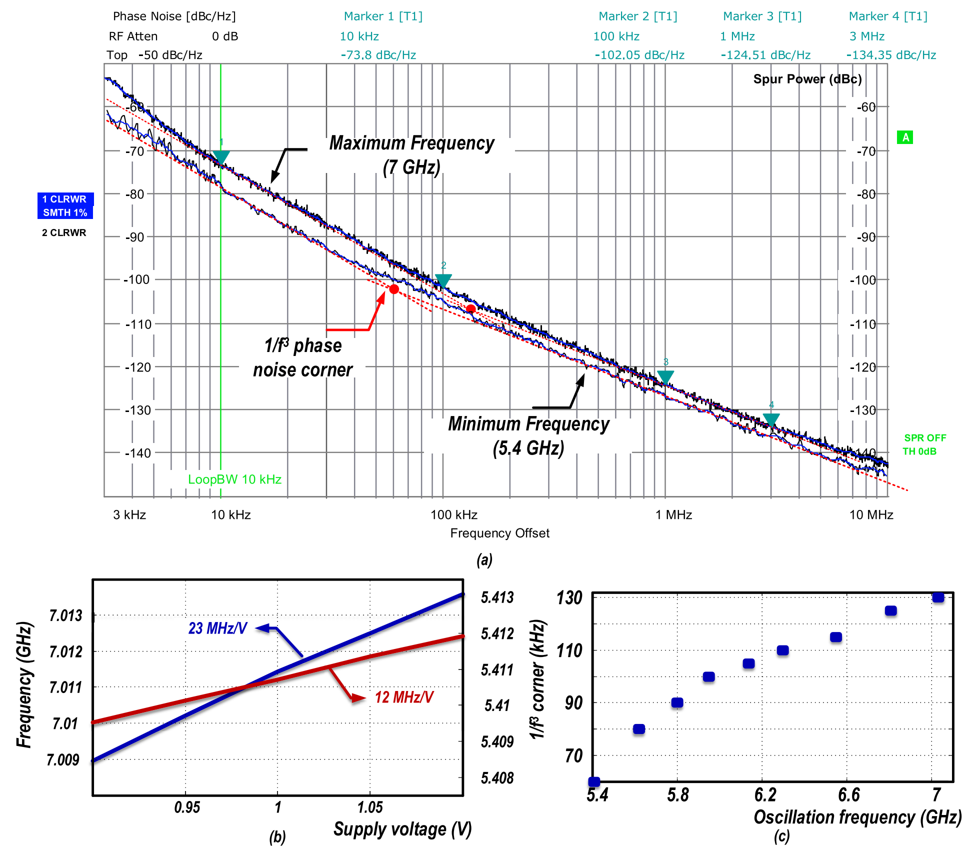

Fig. 17. Class-$F_{2,3}$ oscillator: measured (a) PN at f_{max} and f_{min}, (b) frequency pushing due to supply voltage variation, and (c) $1/f^3$ corner over tuning range.

TABLE I

PERFORMANCE SUMMARY AND COMPARISON WITH RELEVANT OSCILLATORS

		Class-D/F₂		Class-D [4]		Noise Filtering Class-D [4]		**Class-F₂,₃**		Class-F₃[5]	[20]	[25]	[31]
Technology		**40 nm**		65 nm		65 nm		**40 nm**		65 nm	65 nm	28 nm	130 nm
Thick metal		**No**		Yes		Yes		**Yes**		Yes	NA	NA	NA
V_{DD} (V)		**0.5**		0.4		0.4		**1**		1.25	1.2	0.9	1.4
Tuning range (%)		**31**		45		45		**25**		25	18	27.2	1.7
Core area (mm²)		**0.1**		0.12		0.15		**0.13**		0.12	0.08	0.19	0.09
Freq. (GHz)		**f_{min}**	**f_{max}**	f_{min}	f_{max}	f_{min}	f_{max}	**f_{min}**	**f_{max}**	f_{max}	f_{max}	f_{mid}	f_{mid}
		3.3	**4.5**	3	4.8	3	4.8	**5.4**	**7**	7.4	3.6	3.3	2.4
P_{DC} (mW)		**4.1**	**2.5**	6.8	4	6.8	3.6	**12**	**10**	15	0.72	6.8	4.2
PN (dBc /Hz)	100kHz	**-101.2**	**-96.2**	-101	-91	-102	-92.5	**105.3**	**102.1**	-98.5	-94.4	-106	108.4
	1MHz	**-123.4**	**-119**	-127	-119	-128	-121	**126.7**	**124.5**	-125	-114.4	-130	128.4
	10MHz	**-143.4**	**-139**	-149.5	-143.5	-150	-144.5	**146.7**	**144.5**	-147	-134.4	-150	148.4
FoM† (dB)	100kHz	**185.4**	**185.3**	182.2	178.6	183.2	180.6	**189.1**	**188.9**	184.1	187	188.2	189.8
	1MHz	**187.6**	**188**	188.2	186.6	189.2	189.1	**190.5**	**191.4**	190.6	187	192.2	189.8
	10MHz	**187.6**	**188**	190.7	191.1	191.2	192.6	**190.5**	**191.4**	192.6	187	192.2	189.8
$1/f^3$ corner (kHz)		**60**	**100**	800	2100	650	1500	**60**	**130**	700	10	200	<10
Freq. pushing (MHz/V)		**40 @0.5 V**	**60 @0.5 V**	140 @0.5 V	480 @0.5 V	90 @0.5 V	390 @0.5 V	**12 @1V**	**23 @1V**	50 @1.25 V	15 @1.2 V	NA	NA

†FOM= $|PN|+20\log_{10}(\omega_0/\Delta\omega)-10\log_{10}(P_{DC}/1mW)$

frequency mismatch, an 8-b unit-weighted capacitor bank with the LSB of 4 fF is also placed at the primary to tune the DM and CM resonance frequencies. The oscillator is tunable between 5.4 and 7 GHz, and the primary and secondary capacitors are changed simultaneously to preserve the class-$F_{2,3}$ operation. The $M_{1,2}$ transistors are (64/0.27) μm thick-oxide devices to tolerate large voltage swings. The tail resistor R_T bank is realized with a fixed 40 Ω resistor in parallel with 7-b binary-weighted switchable resistors with the LSB size of 5 Ω. This bank can tune the oscillation current from 5 to 20 mA. The chip micrograph is shown in Fig. 15(b); the core die area is 0.12 mm^2.

Fig. 17(a) shows the measured PN of the class-$F_{2,3}$ oscillator at $f_{\max}$ and $f_{\min}$ with $V_{DD} = 1$ V. Current consumption is 10 and 12 mA. The $1/f^3$ corner is 130 kHz at $f_{\max}$ and reduces to ∼60 kHz at $f_{\min}$. The $1/f^3$ corner over TR is plotted in Fig. 17(c). The supply frequency pushing is 23 and 12 MHz/V at $f_{\max}$ and $f_{\min}$, respectively [see Fig. 17(b)]. Table I compares its performance with the original class-F oscillator. Compared with the original design, FoM is degraded about 1–2 dB at the 10 MHz offset, which is due to the tail resistor loading the tank more than the tail transistor originally, thus degrading PN slightly. Despite this degradation, FoM at 100 kHz is enhanced by at least 4 dB, and the $1/f^3$ corner is improved five times.

V. Conclusion

This paper presented a technique to reduce a 1/f noise upconversion in a harmonically rich tank current. We showed that when even-order harmonics of the tank current flow into the capacitive part of the tank, they distort the oscillation waveform by making its rise and fall times asymmetric and, hence, causing the 1/f noise upconversion. Odd-order harmonics also distort the oscillation waveform; however, the waveform in that case is still symmetric and will not result in the 1/f noise upconversion. We proposed to design a ω_0-tank that shows an auxiliary CM resonant peak at $2\omega_0$, which is the main contributor to the 1/f noise upconversion, and showed how oscillation waveform becomes symmetric by the auxiliary resonance. We described how to realize the F_2-tank without the die area penalty, by taking advantage of different properties of inductors and transformers in DM and CM excitations. Class-D/F_2 and class-$F_{2,3}$ oscillators employing, respectively, inductor and transformer-based F_2 tanks are designed in 40 nm CMOS to show the effectiveness of our proposed method. The $1/f^3$ corner improves ten times in class-D/F_2 and five times in class-$F_{2,3}$ versus their original counterparts.

VI. Acknowledgment

The authors would like to thank Atef Akhnoukh, Wil Straver, Ali Kaichouhi, Gerasimos Vlachogiannakis and Zhirui Zong from TU Delft for measurement support and technical discussions and RF Department of Hisilicon in Shanghai for their support.

References

[1] H. Darabi, H. Jensen, and A. Zolfaghari, "Analysis and design of small-signal polar transmitters for cellular applications," *IEEE J. Solid-State Circuits*, vol. 46, no. 6, pp. 1237–1249, Jun. 2011.

[2] D. Tasca, M. Zanuso, G. Marzin, S. Levantino, C. Samori, and A. L. Lacaita, "A 2.9–4.0-GHz fractional-N digital PLL with bang-bang phase detector and 560-fs_{rms} integrated jitter at 4.5-mW power," *IEEE J. Solid-State Circuits*, vol. 46, no. 12, pp. 2745–2758, Dec. 2011.

[3] L. Fanori and P. Andreani, "Highly efficient class-C CMOS VCOs, including a comparison with class-B VCOs," *IEEE J. Solid-State Circuits*, vol. 48, no. 7, pp. 1730–1740, Jul. 2013.

[4] L. Fanori and P. Andreani, "Class-D CMOS oscillators," *IEEE J. Solid-State Circuits*, vol. 48, no. 12, pp. 3105–3119, Dec. 2013.

[5] M. Babaie and R. B. Staszewski, "A class-F CMOS oscillator," *IEEE J. Solid-State Circuits*, vol. 48, no. 12, pp. 3120–3133, Dec. 2013.

[6] E. Hegazi and A. A. Abidi, "Varactor characteristics, oscillator tuning curves, and AM-FM conversion," *IEEE J. Solid-State Circuits*, vol. 38, no. 6, pp. 1033–1039, Jun. 2003.

[7] B. Soltanian and P. Kinget, "AM-FM conversion by the active devices in MOS LC-VCOs and its effect on the optimal amplitude," in *Proc. IEEE Radio Freq. Integr. Circuits Symp.*, Jun. 2006, pp. 104–108.

[8] S. Levantino, C. Samori, A. Bonfanti, S. L. J. Gierkink, A. L. Lacaita, and V. Boccuzzi, "Frequency dependence on bias current in 5 GHz CMOS VCOs: Impact on tuning range and flicker noise upconversion," *IEEE J. Solid-State Circuits*, vol. 37, no. 8, pp. 1003–1011, Aug. 2002.

[9] J. Groszkowski, "The interdependence of frequency variation and harmonic content, and the problem of constant-frequency oscillators," *Proc. Inst. Radio Eng.*, vol. 21, no. 7, pp. 958–981, Jul. 1933.

[10] A. Bevilacqua and P. Andreani, "On the bias noise to phase noise conversion in harmonic oscillators using Groszkowski theory," in *Proc. IEEE Int. Symp. Circuits Syst.*, May 2011, pp. 217–220.

[11] J. J. Rael and A. A. Abidi, "Physical processes of phase noise in differential LC oscillators," in *Proc. IEEE Custom Integr. Circuits Conf.*, Sep. 2000, pp. 569–572.

[12] A. Hajimiri and T. H. Lee, "A general theory of phase noise in electrical oscillators," *IEEE J. Solid-State Circuits*, vol. 33, no. 2, pp. 179–194, Feb. 1998.

[13] J. E. Post, Jr., I. R. Linscott, and M. H. Oslick, "Waveform symmetry properties and phase noise in oscillators," *Electron. Lett.*, vol. 34, no. 16, pp. 1547–1548, Aug. 1998.

[14] D. Murphy, J. J. Rael, and A. A. Abidi, "Phase noise in LC oscillators: A phasor-based analysis of a general result and of loaded Q," *IEEE Trans. Circuits Syst. I, Reg. Papers*, vol. 57, no. 6, pp. 1187–1203, Jun. 2010.

[15] A. Bevilacqua and P. Andreani, "An analysis of $1/f$ noise to phase noise conversion in CMOS harmonic oscillators," *IEEE Trans. Circuits Syst. I, Reg. Papers*, vol. 59, no. 5, pp. 938–945, May 2012.

[16] E. A. Vittoz, M. G. R. Degrauwe, and S. Bitz, "High-performance crystal oscillator circuits: Theory and application," *IEEE J. Solid-State Circuits*, vol. 23, no. 3, pp. 774–783, Jun. 1988.

[17] M. A. Margarit, J. L. Tham, R. G. Meyer, and M. J. Deen, "A low-noise, low-power VCO with automatic amplitude control for wireless applications," *IEEE J. Solid-State Circuits*, vol. 34, no. 6, pp. 761–771, Jun. 1999.

[18] A. Jerng and C. G. Sodini, "The impact of device type and sizing on phase noise mechanisms," *IEEE J. Solid-State Circuits*, vol. 40, no. 2, pp. 360–369, Feb. 2005.

[19] S.-J. Yun, C.-Y. Cha, H.-C. Choi, and S.-G. Lee, "RF CMOS *LC*-oscillator with source damping resistors," *IEEE Microw. Wireless Compon. Lett.*, vol. 16, no. 9, pp. 511–513, Sep. 2006.

[20] F. Pepe, A. Bonfanti, S. Levantino, C. Samori, and A. L. Lacaita, "Suppression of flicker noise up-conversion in a 65-nm CMOS VCO in the 3.0-to-3.6 GHz band," *IEEE J. Solid-State Circuits*, vol. 48, no. 10, pp. 2375–2389, Oct. 2013.

[21] A. Bonfanti, F. Pepe, C. Samori, and A. L. Lacaita, "Flicker noise up-conversion due to harmonic distortion in Van der Pol CMOS oscillators," *IEEE Trans. Circuits Syst. I, Reg. Papers*, vol. 59, no. 7, pp. 1418–1430, Jul. 2012.

[22] F. Pepe, A. Bonfanti, S. Levantino, C. Samori, and A. L. Lacaita, "Analysis and minimization of flicker noise up-conversion in voltage-biased oscillators," *IEEE Trans. Microw. Theory Techn.*, vol. 61, no. 6, pp. 2382–2394, Jun. 2013.

[23] M. Shahmohammadi, M. Babaie, and R. B. Staszewski, "A $1/f$ noise upconversion reduction technique applied to class-D and class-F oscillators," in *IEEE Int. Solid-State Circuits Conf. (ISSCC) Dig. Tech. Papers*, Feb. 2015, pp. 444–445.

[24] P. Andreani, X. Wang, L. Vandi, and A. Fard, "A study of phase noise in Colpitts and LC-tank CMOS oscillators," *IEEE J. Solid-State Circuits*, vol. 40, no. 5, pp. 1107–1118, May 2005.

[25] D. Murphy, H. Darabi, and H. Wu, "A VCO with implicit common-mode resonance," in *IEEE Int. Solid-State Circuits Conf. (ISSCC) Dig. Tech. Papers*, Feb. 2015, pp. 442–443.

[26] J. Chen *et al.*, "A digitally modulated mm-wave Cartesian beamforming transmitter with quadrature spatial combining," in *IEEE Int. Solid-State Circuits Conf. (ISSCC) Dig. Tech. Papers*, Feb. 2013, pp. 232–233.

[27] D. Chowdhury, L. Ye, E. Alon, and A. M. Niknejad, "An efficient mixed-signal 2.4-GHz polar power amplifier in 65-nm CMOS technology," *IEEE J. Solid-State Circuits*, vol. 46, no. 8, pp. 1796–1809, Aug. 2011.

[28] M. Babaie and R. B. Staszewski, “An ultra-low phase noise class-F_2 CMOS oscillator with 191 dBc/Hz FoM and long-term reliability,” *IEEE J. Solid-State Circuits*, vol. 50, no. 3, pp. 679–692, Mar. 2015.

[29] A. Mazzanti and A. Bevilacqua, “On the phase noise performance of transformer-based CMOS differential-pair harmonic oscillators,” *IEEE Trans. Circuits Syst. I, Reg. Papers*, vol. 62, no. 9, pp. 2334–2341, Sep. 2015.

[30] E. Hegazi, H. Sjoland, and A. A. Abidi, “A filtering technique to lower LC oscillator phase noise,” *IEEE J. Solid-State Circuits*, vol. 36, no. 12, pp. 1921–1930, Dec. 2001.

[31] A. Mostajeran, M. S. Bakhtiar, and E. Afshari, “A 2.4GHz VCO with FOM of 190 dBc/Hz at 10 kHz-to-2 MHz offset frequencies in 0.13 μm CMOS using an ISF manipulation technique,” in *IEEE Int. Solid-State Circuits Conf. (ISSCC) Dig. Tech. Papers*, Feb. 2015, pp. 452–453.

Mina Shahmohammadi (S’12) received the B.Sc. degree in communication systems from the Amirkabir University of Technology, Tehran, Iran, in 2005, and the M.Sc. degree in electronics from the University of Tehran, Tehran, in 2007. She is currently pursuing the Ph.D. degree with Delft University of Technology, Delft, The Netherlands.

From 2007 to 2011, she was with Rezvan Engineering Co., Tehran, Iran, as an Analog Designer. She was a Research Assistant with the Electronic Instrumentation Laboratory, Delft University of Technology from 2011 to 2013, where she was involved in resistor based temperature sensors. She joined the Electronics Research Laboratory, Delft University of Technology in 2013. Her current research interests include analog and RF integrated circuit design.

Masoud Babaie (S’12–M’16) received the B.Sc. (with highest honors) and M.Sc. degrees in electrical engineering from the Amirkabir University of Technology, Tehran, Iran, and the Sharif University of Technology, Tehran, in 2004 and 2006, respectively, and the Ph.D. (*cum laude*) degree from the Delft University of Technology, Delft, the Netherlands, in 2016.

He joined the Kavoshcom Research and Develpment Group, Tehran, in 2006, where he was involved in designing tactical communication systems. He was appointed a CTO of the company from 2009 to 2011. He was consulting of the RF Group with TSMC, Hsinchu, Taiwan, from 2013 to 2015, where he was involved in designing 28 nm all-digital PLL and Bluetooth low-energy transceiver chips. From 2014 to 2015, he was a Visiting Scholar Researcher with Berkeley Wireless Research Center, Berkeley, CA, USA, with the Group of Prof. A. Niknejad. In August 2016, he has joined the Delft University of Technology as an Assistant Professor. His current research interests include analog and RF/mm-wave integrated circuits and systems for wireless communications.

Dr. Babaie serves as a Reviewer of the IEEE JOURNAL OF SOLID-STATE CIRCUITS. He was a recipient of the IEEE Solid-State Circuits Society (SSCS) Pre-doctoral Achievement Award from 2015 to 2016.

Robert Bogdan Staszewski (M’97–SM’05–F’09) was born in Bialystok, Poland. He received the B.Sc. (*summa cum laude*), M.Sc., and Ph.D. degrees from the University of Texas at Dallas, Dallas, TX, USA, in 1991, 1992 and 2002, respectively, all in electrical engineering.

From 1991 to 1995, he was with Alcatel Network Systems, Richardson, TX, USA, where he was involved in SONET cross-connect systems for fiber optics communications. He joined Texas Instruments, Dallas, TX, USA, in 1995, where he was elected Distinguished Member of Technical Staff (limited to 2% of Technical Staff). From 1995 to 1999, he was involved in advanced CMOS read channel development for hard disk drives. In 1999, he co-started a Digital RF Processor (DRP) Group with in Texas Instruments with a mission to invent new digitally intensive approaches to traditional RF functions for integrated radios in deeply-scaled CMOS processes. He was appointed as a CTO of the DRP Group from 2007 to 2009. In 2009, he joined Delft University of Technology, Delft, The Netherlands, where he is currently a part-time Full Professor. Since 2014, he has been a Professor with University College Dublin, Dublin, Ireland. He has authored or co-authored three books, four book chapters, 200 journal and conference publications, and holds 160 issued U.S. patents. His current research interests include nanoscale CMOS architectures and circuits for frequency synthesizers, transmitters, and receivers.

Prof. Staszewski has been a TPC member of International Solid-State Circuits Conference, RFIC, ESSCIRC, ISCAS and RFIT. He is a recipient of the IEEE Circuits and Systems Industrial Pioneer Award.